Science
AAAS

Evidence for a Polar Ethane Cloud on Titan
C. A. Griffith, *et al.*
Science **313**, 1620 (2006);
DOI: 10.1126/science.1128245

2. G. Scoles, Ed., *Atomic and Molecular Beam Methods* (Oxford Univ. Press, New York, 1988), vol. 1.
3. G. Scoles, Ed., *Atomic and Molecular Beam Methods* (Oxford Univ. Press, New York, 1992), vol. 2.
4. T. P. Rakitzis, A. J. van den Brom, M. H. M. Janssen, *Science* **303**, 1852 (2004).
5. X. Liu, J. J. Lin, S. Harich, G. C. Schatz, X. Yang, *Science* **289**, 1536 (2000).
6. S. A. Harich *et al.*, *Nature* **419**, 281 (2002).
7. J. J. Lin, J. Zhou, W. Shiu, K. Liu, *Science* **300**, 966 (2003).
8. J. J. van Leuken, J. Bulthuis, S. Stolte, J. G. Snijders, *Chem. Phys. Lett.* **260**, 595 (1996).
9. R. N. Zare, *Science* **279**, 1875 (1998).
10. M. C. van Beek, G. Berden, H. L. Bethlem, J. J. ter Meulen, *Phys. Rev. Lett.* **86**, 4001 (2001).
11. G. Hall, K. Liu, M. J. McAuliffe, C. F. Giese, W. R. Gentry, *J. Chem. Phys.* **78**, 5260 (1983).
12. R. G. Macdonald, K. Liu, *J. Chem. Phys.* **91**, 821 (1989).
13. D. M. Sonnenfroh, R. G. Macdonald, K. Liu, *J. Chem. Phys.* **94**, 6508 (1991).
14. R. T. Skodje *et al.*, *Phys. Rev. Lett.* **85**, 1206 (2000).
15. D. Skouteris *et al.*, *Science* **286**, 1713 (1999).
16. W. Shiu, J. J. Lin, K. Liu, *Phys. Rev. Lett.* **92**, 103201 (2004).
17. R. C. Forrey, N. Balakrishnan, V. Kharchenko, A. Dalgarno, *Phys. Rev. A.* **58**, R2645 (1998).
18. N. Balakrishnan, A. Dalgarno, R. C. Forrey, *J. Chem. Phys.* **113**, 621 (2000).
19. C. D. Ball, F. C. De Lucia, *Phys. Rev. Lett.* **81**, 305 (1998).
20. I. R. Sims *et al.*, *J. Chem. Phys.* **97**, 8798 (1992).
21. P. Staanum, S. D. Kraft, J. Lange, R. Wester, M. Weidemüller, *Phys. Rev. Lett.* **96**, 023201 (2006).
22. N. Zahzam, T. Vogt, M. Mudrich, D. Comparat, P. Pillet, *Phys. Rev. Lett.* **96**, 023202 (2006).
23. C. E. Heiner, H. L. Bethlem, G. Meijer, *Phys. Chem. Chem. Phys.* **8**, 2666 (2006) and references therein.
24. L. T. Cowley, M. A. D. Fluendy, K. P. Lawley, *Rev. Sci. Instrum.* **41**, 666 (1970).
25. H. L. Bethlem, G. Berden, G. Meijer, *Phys. Rev. Lett.* **83**, 1558 (1999).
26. H. L. Bethlem, G. Meijer, *Int. Rev. Phys. Chem.* **22**, 73 (2003).
27. The labels $X^2\Pi_{3/2}$, v, and J indicate the electronic, vibrational, and rotational state of the OH radical, respectively. The spectroscopic symmetry labels e and f refer to the total parity of the electronic wavefunction, exclusive of rotation.
28. M. C. van Beek, J. J. ter Meulen, M. H. Alexander, *J. Chem. Phys.* **113**, 628 (2000).
29. M. C. van Beek, J. J. ter Meulen, M. H. Alexander, *J. Chem. Phys.* **113**, 637 (2000).
30. S. Y. T. van de Meerakker, N. Vanhaecke, G. Meijer, *Annu. Rev. Phys. Chem.* **57**, 159 (2006).
31. M. H. Alexander, *J. Chem. Phys.* **76**, 5974 (1982).
32. P. J. Knowles, C. Hampel, H.-J. Werner, *J. Chem. Phys.* **99**, 5219 (1993).
33. MOLPRO, version 2002.6, a package of ab initio programs, H. J. Werner, P. J. Knowles, R. Lindh, F. R. Manby, M. Schütz, and others, Cardiff, UK (www.molpro.net).
34. K. A. Peterson, D. Figgen, E. Goll, H. Stoll, M. Dolg, *J. Chem. Phys.* **119**, 11113 (2003).
35. G. Dhont, W. B. Zeimen, G. C. Groenenboom, A. van der Avoird, *J. Chem. Phys.* **120**, 103 (2004).
36. E. P. Wigner, *Phys. Rev.* **73**, 1002 (1948).
37. The validity of this assumption is verified by analytically modeling the detection probability in the limiting cases of forward, backward, and isotropic scattering. The difference is found to be within the error bars of our data.
38. G. C. Groenenboom, N. Balakrishnan, *J. Chem. Phys.* **118**, 7380 (2003).
39. T.-S. Ho, H. Rabitz, *J. Chem. Phys.* **104**, 2584 (1996).

40. This research is supported by the European Union Cold Molecules Network. We thank N. Vanhaecke for help preparing this experiment and D. W. Chandler for many fruitful discussions and for carefully reading the manuscript.

Supporting Online Material

www.sciencemag.org/cgi/content/full/313/5793/1617/DC1
Computer Codes

28 June 2006; accepted 7 August 2006
10.1126/science.1131867

Evidence for a Polar Ethane Cloud on Titan

C. A. Griffith,[1]* P. Penteado,[1] P. Rannou,[2] R. Brown,[1] V. Boudon,[3] K. H. Baines,[4] R. Clark,[5] P. Drossart,[6] B. Buratti,[4] P. Nicholson,[7] C. P. McKay,[8] A. Coustenis,[6] A. Negrao,[2,9] R. Jaumann[10]

Spectra from Cassini's Visual and Infrared Mapping Spectrometer reveal the presence of a vast tropospheric cloud on Titan at latitudes 51° to 68° north and all longitudes observed (10° to 190° west). The derived characteristics indicate that this cloud is composed of ethane and forms as a result of stratospheric subsidence and the particularly cool conditions near the moon's north pole. Preferential condensation of ethane, perhaps as ice, at Titan's poles during the winters may partially explain the lack of liquid ethane oceans on Titan's surface at middle and lower latitudes.

Past images of Saturn's largest moon, Titan, display large clouds only where solar heating is greatest, which presently occurs at high southern latitudes (*1*–*3*). The morphology of Titan's southern clouds indicates that they are convective, composed of methane, and result from the summer heating of Titan's surface and updrafts from Titan's summer Hadley cell (*1*, *4*–*6*). Similar processes instigate the formation of thunderstorms on Earth. The latent heat of Titan's major condensable constituent, methane, is large enough that, like water on Earth, adiabatic lifting and consequent cooling of air cause cloud formation (*7*). In contrast, at high northern latitudes, air circulates downward from the dry stratosphere (above an altitude of 40 km) and is heated through compression, which prevents the formation of methane clouds.

Spectral images of Titan's northern hemisphere, recorded by Cassini's Visual and Infrared Mapping Spectrometer (VIMS) (*8*), indicate a ubiquitous bright band at 51° to 68°N latitude, at the edge of Titan's arctic circle (Fig. 1). Its presence at higher latitudes cannot be determined because of a lack of illumination. The band appears at wavelengths that detect altitudes above 30 km (1.9, 2.13, and 2.7 to 2.9 μm) yet not at wavelengths that probe altitudes above 60 km (for example, at 1.67, 2.25, and 3.2 μm), indicating that particles near an altitude of 40 km are the cause (Fig. 2). Unlike Titan's southern clouds, this northern cloud shows no hourly variability and is diffusely spread over a large area, with only small continuous variations in optical depth between adjacent pixels (Fig. 1).

The cloud appears at latitudes where Titan's general circulation concentrates and transports photochemical products, principally ethane, to lower altitudes, where they condense and may form clouds (*6*). Methane (the second most abundant atmospheric constituent after nitrogen) is dissociated irreversibly by solar ultraviolet light, producing primarily ethane and, at one-sixth and one-10th of the ethane production rate, respectively, acetylene and haze, as well as other less abundant organic molecules (*9*, *10*). These photochemical by-products precipitate to Titan's surface. Titan's atmospheric composition and photochemical models indicate that ethane accumulates as a liquid (at the equatorial surface temperature of 93.5 K) at a rate of ~300 m (if global) over Titan's lifetime of 4.5 billion years, whereas solid sediments, including acetylene and haze particles, accumulate at roughly one-third of this rate (*10*). Thus, unless methane is a recent addition to Titan's atmosphere (*11*) or ethane incorporates itself into surface solids (*12*), it has been reasoned that a considerable fraction of the surface should be covered with liquid ethane (*13*). Titan's surface reveals dunes of solid sediments, probably including haze particles and acetylene ice (*14*). In addition, the surface is riddled with alluvial features (*15*–*17*), suggesting the occurrence of methane rain in the past. Craters are rare, indicating geological relaxation as well as their burial by photochemical sediments (*15*, *16*, *18*). Yet Titan appears depleted of its most abundant photochemical by-product. Except for the ethane-damp surface measured by Huygens (*19*), no condensed form of ethane has been detected (*20*), despite its rapid production in Titan's stratosphere and

[1]Lunar and Planetary Laboratory, University of Arizona, Tucson, AZ, 85721 USA. [2]Service d'Aéronomie, Université de Versailles-St-Quentin, BP3, 91371 Verriéres le Buisson, France. [3]Laboratoire de Physique de l'Université de Bourgogne, CNRS UMR 5027, Boîte Postale 47870, F-21078 Dijon, France. [4]Jet Propulsion Laboratory, California Institute of Technology, Pasadena, CA, 91109 USA. [5]U.S. Geological Survey, Denver, CO, 80225 USA. [6]Observatoire de Paris, 5 Place Jules Jannsen, Meudon, France. [7]Department of Astronomy, Cornell University, Ithaca, NY, USA. [8]National Aeronautics and Space Administration, Ames Research Center, Moffett Field, Mountain View, CA, USA. [9]Observatório Astronómico de Lisboa, 1349–018 Lisboa, Portugal. [10]Institute of Planetary Exploration, Deutsche Zentrum für Luft- und Raumfahrt, Germany.

the expectation of finding ethane-rich oceans before the Cassini encounter (*13*).

To determine the nature of Titan's northern cloud, whether it formed from methane or from the condensation of ethane and other photochemical by-products, we primarily analyzed the 2- to 2.5-μm, 2.8- to 3.2-μm, and 4.9- to 5.1-μm wavelength regions of VIMS' 0.88- to 5.11-μm spectra, which provide the clearest views down to the troposphere (*21*). The radiative transfer equation was solved with the discrete-ordinates approximation to simulate the absorption and scattering of Titan's atmosphere and surface (*22*). We first constrained the optical depths of the gases and haze above the clouds. We quantified methane absorption with line-by-line techniques (*5*) and new methane line parameters at 2.8 to 3.2 μm (*23*, *24*) and calculated pressure-induced H_2 and N_2 absorption using laboratory data (*25*). Real and imaginary indices of refraction of 1.35 and 0.0001, respectively, for ethane were assumed at both 2.1- and 2.9-μm wavelengths (*26*). We also assumed the presence of spherical haze particles having radii of 0.2 μm from altitudes of 180 to 90 km. Below 90 km, radii increase with atmospheric pressure to 0.8 μm at the altitude of 40 km (*5*). Analyses of the cloudless 2.1- to 2.2-μm spectra indicate a haze profile whose density decreases with altitude, with a scale height of 60 km above an altitude of 100 km; a particle density of 21 cm^{-3} at 130 km; and a constant density of 30 cm^{-3} from an altitude of 90 to 100 km, 9 cm^{-3} from 70 to 90 km, and 1 cm^{-3} from 30 to 70 km. Although other profiles also match the data, we can accurately estimate the haze optical depth above the cloud (0.16 at 2.1 μm), because it considerably exceeds the gas optical depth (0.05). A comparison of the calculations to the observed slope of Titan's 2.11- to 2.18-μm spectra provided the cloud heights (*5*). The 2.0-, 2.8-, and 5.0-μm albedos indicated the cloud optical depths. These values allowed us to estimate the size of the cloud particles (*5*) and their column mass, which provide clues to the formation and composition of Titan's northern cloud.

We analyzed the spectra lying within the 48° to 55°N latitude band that were farthest from the terminator and thus most directly illuminated by the Sun. The cloud was found to reside at altitudes of 30 to 50 km, with no trace of clouds above 60 km (Fig. 2), suggesting that we were not simply observing the low-altitude sedimentation of Titan's stratospheric hazes and condensates (*27*, *28*). At 55°N latitude, the cloud's optical depth was 0.06 ± 0.01 at both 2.1- and 2.9-μm wavelengths, assuming the optical constants of ethane. The error quoted above (0.01) refers to the 3σ standard deviation that results from noise. If the optical constants of haze are assumed, we derive optical depths

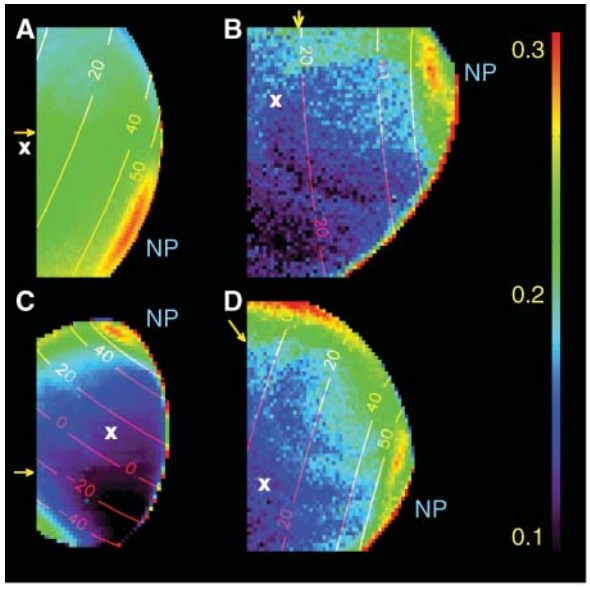

Fig. 1. Titan's 2.8-μm albedo, multiplied by the function $(\mu + \mu_o)/\mu_o^{0.3}$ (where μ_o and μ are the cosines of the illumination and emission angles), to lessen effects due to differences in illumination across the disk, indicates a cloud (red area) near 56°N. The cloud appears at all west longitudes observed: 115° to 190° (**A**), 10° to 118° [(**B**) and (**C**)], and 25° to 95° (**D**). Sunlight scattering off the limb (referred to as limb brightening) also appears red in (D). Titan's tilt prevents the illumination of latitudes exceeding 70°N. The pixel resolution (horizontal by vertical) is in the range from (50 to 95) by (50 to 150) km^2. Images were recorded at 6:26 universal time (UT) 13 December 2004 (A), 4:25 UT 22 August 2005 (B), 23:44 UT 21 August 2005 (C), and 2:55 UT 7 September 2005 (D). NP, direction of the north pole; x, subspacecraft point; yellow arrow, direction of solar illumination.

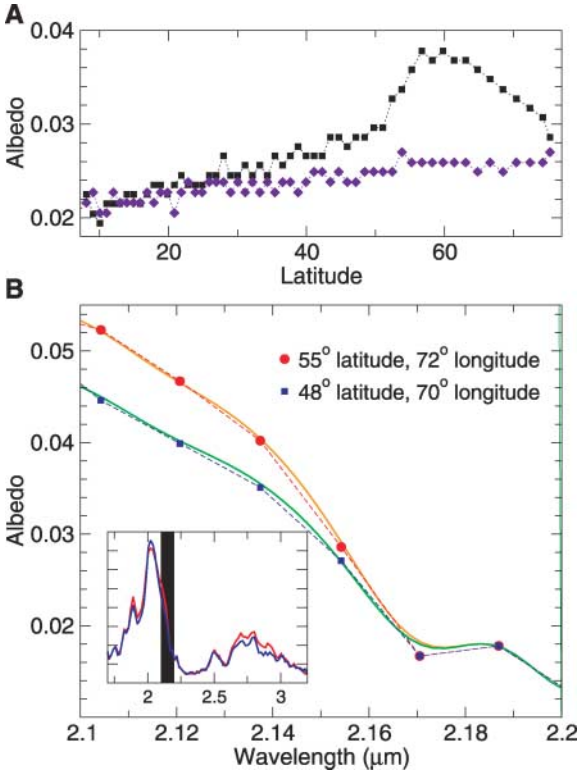

Fig. 2. (**A**) The change in Titan's albedo with latitude, made from a horizontal cut (at the 19th pixel row from the top) through the image in Fig. 1B at wavelengths of 2.11 μm (black squares) and 2.17 μm (purple diamonds), which probe the 30- to 50-km and 60- to 80-km altitude ranges, respectively. The cloud band appears north of 51°N latitude at 2.11 μm but not at 2.17 μm. (**B**) VIMS spectra recorded within (red circles) and outside of (blue squares) the bright cloud band (recorded at 23:04 UT 21 August 2005) are compared to calculated spectra that assume the absence of a cloud (green line) and the presence of a cloud at an altitude of 40 km of optical depth 0.02 (orange line). (**Inset**) The same observations shown over a larger wavelength region than that modeled in (B) (black rectangle) indicate increased brightness due to the cloud at wavelengths (1.9, 2.13, and 2.7 to 2.9 μm) that detect the tropopause. At 2 μm, the surface is visible and, for this pair of spectra, more highly reflective from cloudless terrain than cloudy terrain. The spectral resolution is 0.017 μm.

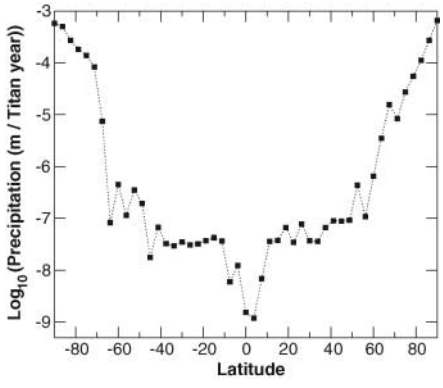

Fig. 3. The yearly average precipitation of ethane (dashed line) according to the GCM model of Rannou *et al.* (*6*). The downwelling circulation branch surrounding the poles during the winters causes ethane to descend from the stratosphere to the tropopause, where it condenses and precipitates to the surface. Consequently, ethane is predicted to accumulate in Titan's polar regions.

of 0.06 ± 0.01 at 2.1 μm and 0.12 ± 0.01 at 2.9 μm. Near 1.64 μm, VIMS spectra are corrupted because of a filter gap (*8*). The remaining spectral windows, 0.94, 1.08, and 1.28 μm, did not display albedo changes from the cloud, because the two-way optical depth to the cloud altitude exceeds unity, which is a result of the oblique solar illumination and the high scattering efficiency of the haze. We found that a cloud of optical depth 0.1 at 2.9 μm would be imperceptible at these lower wavelengths for particles larger than 1 μm. At 5 μm, Titan's haze scatters inefficiently, with an optical depth of less than 0.1. Yet no cloud signature was detected, indicating cloud optical depths smaller than 0.01. This constraint, taken together with the optical depths at 2.1 and 2.9 μm, indicates that the particle sizes were smaller than 3 μm. Thus, the effective radius of the cloud particles is 1 to 3 μm.

Titan's northern cloud consists of smaller particles than those composing the methane clouds in the south, whose radii exceed 10 μm. Particles with radii exceeding 50 μm are expected from methane condensation as a result of Titan's low density of nucleation sites, coupled with methane's high mixing ratio (*29*). The large southern particles suggest that in the north, where atmospheric conditions are similar, methane condensation similarly leads to particles with radii exceeding 50 μm. The small particle sizes thus suggest the condensation of a less abundant species.

Both the cloud's altitude and latitude agree with the predicted concentration of Titan's haze, which is expected to peak at an altitude of roughly 35 km poleward of ~60°N latitude, based on a recent general circulation model (GCM) (*6*). However, the optical constants of Titan's haze disagree with the cloud's spectral features. Haze particles are dark at 2.9 μm, unlike the observed cloud feature; consequently, two times more haze particles are needed to reproduce the cloud feature at 2.9 μm than at 2.1 μm, which is an unphysical result. The optical properties indicate that the cloud is not produced by a concentration of haze but rather by local condensation.

The characteristics of Titan's northern cloud are all consistent with the condensation of ethane. The cloud's 2.1- and 2.9-μm albedos can both be explained as resulting from a column of ~60,000 cm^{-2} of ethane particles having radii of 3 μm. The mass column abundance, $\sim 4 \times 10^{-6}$ g cm^{-2}, matches estimates at 60°N latitude from GCM models (*6*). The altitude of the cloud agrees with that expected for the winter subsidence of ethane, having a mixing ratio of $2.2 \pm 0.5 \times 10^{-5}$ at an altitude of ~150 km (*9*, *30*) and assuming the equatorial temperature profile (*6*, *31*). In addition, the particle sizes agree with those expected for high ethane condensates, given the abundance of ethane and the number density of nucleation sites (*6*, *32*). The unvarying nature of the cloud results from the slow vertical fall rate, which is 3 km per month for particles with radii of 2 μm (*32*).

The southern edge of Titan's cirrus cloud region occurs at the latitude north of which GCM models predict the descent of air from the stratosphere to the troposphere. Ethane, which is undersaturated at altitudes above ~65 km, descends to 30 to 50 km (where its mixing ratio exceeds saturation by a factor of several hundred) and condenses to form a cirrus cloud surrounding the pole. This explanation implies that we are observing the edge of a massive polar ethane cloud and the preferential condensation, sedimentation, and surface accumulation of ethane within 35° of Titan's poles (Fig. 3). Here, temperatures are expected to drop below the freezing point of pure ethane (90.3 K) during the winter and, depending on the haze opacity, possibly throughout most of Titan's year (*6*, *33*). If conditions remain cool enough throughout the year, Titan may accumulate ethane ice each winter at the poles and develop year-round polar caps.

An ethane cloud probably contains haze and other photochemically produced ices (such as acetylene), which condense mainly at altitudes of 65 to 90 km and mix downward to form part of the cirrus cloud (*27*, *28*). Additionally, methane and dissolved N_2 may condense on the ethane particles. Yet at the tropopause, methane is presently probably subsaturated because of the subsidence of air from the dry stratosphere (*6*). We detected no evidence for methane condensation resulting from meteorological methane fluctuations and temperature variations, which are spatially variable effects. The cloud is markedly uniform, without evident regions of methane-coated particles with radii exceeding 5 μm, which would have been detected in the 5-μm images, and without density variations resulting from the faster fall velocities of larger particles. Further investigations will better constrain the cloud composition, including Cassini VIMS measurements to be conducted during the close passes of the moon later in Titan's spring, when the north pole is better illuminated.

Presently, there is no direct evidence of polar caps composed of ethane. The northern pole has not been imaged. Cassini images of the southern pole do not indicate the morphology of 2 km of ethane ice, assuming current rates of ethane production over the past 4.5 billion years, accumulated within 35° of the poles. Yet south polar images suggest flow features, possibly associated with a smaller quantity of ethane ice accumulated on the young surface. The detection of surficial ethane ice is hindered by the correlation of ethane features and methane signatures, which obscure the visibility of Titan's surface. In addition, the polar surface is probably distinct and varied. Similarly, other hydrocarbons would precipitate preferentially at the poles and pollute the ethane ice, and any lowland methane lakes would dissolve and melt ethane, because the mixture's eutectic temperature is 72.5 K (*34*). Such lakes might condense out of Titan's humid lower troposphere during winter. The surface distribution of liquid or solid ethane, whether corralled into the polar regions by circulation or transported by surface flows to lower latitudes, will be determined with radar and near-infrared images of the geomorphology, radio determinations of the polar temperatures, and infrared measurements of the polar composition, which are scheduled for future Cassini encounters with Titan.

References and Notes

1. M. E. Brown, A. H. Bouchez, C. A. Griffith, *Nature* **420**, 795 (2002).
2. H. G. Roe, I. de Pater, B. A. Macintosh, C. P. McKay, *Astrophys. J.* **581**, 1399 (2002).
3. H. G. Roe, A. H. Bouchez, C. A. Trujillo, E. L. Schaller, M. E. Brown, *Astrophys. J.* **618**, L49 (2005).
4. C. A. Griffith, J. L. Hall, T. R. Geballe, *Science* **290**, 509 (2000).
5. C. A. Griffith *et al.*, *Science* **310**, 474 (2005).
6. P. Rannou, F. Montmessin, F. Hourdin, S. Lebonnois, *Science* **311**, 201 (2006).
7. J. E. McDonald, *J. Atmos. Sci.* **21**, 76 (1964).
8. R. Brown *et al.*, *Icarus* **164**, 461 (2003).
9. A. Coustenis, B. Bézard, *Icarus* **115**, 126 (1995).
10. Y. L. Yung, M. Allen, J. P. Pinto, *Astrophys. J. Suppl. Ser.* **55**, 465 (1984).
11. G. Tobie, J. I. Lunine, C. Sotin, *Nature* **440**, 61 (2006).
12. J. P. Osegovic, M. D. Max, *J. Geophys. Res.* **110**, 8004 (2005).
13. J. I. Lunine, D. J. Stevenson, Y. L. Yung, *Science* **222**, 1229 (1983).
14. R. Lorenz *et al.*, *Science* **312**, 724 (2006).
15. C. C. Porco *et al.*, *Nature* **434**, 159 (2005).
16. C. Elachi *et al.*, *Science* **308**, 970 (2005).
17. M. G. Tomasko *et al.*, *Nature* **438**, 765 (2005).
18. J. I. Lunine, N. Artemieva, R. Lorenz, E. Flamini, paper presented at the 36th Annual Lunar and Planetary Science Conference, League City, TX, 14 to 18 March 2005, abstract 1504.
19. H. B. Niemann *et al.*, *Nature* **438**, 779 (2005).
20. R. A. West, M. E. Brown, S. V. Salinas, A. H. Bouchez, H. G. Roe, *Nature* **436**, 670 (2005).
21. C. A. Griffith, T. Owen, T. R. Geballe, J. Rayner, P. Rannou, *Science* **300**, 628 (2003).
22. K. Stamnes, S. Tsay, K. Jayweera, W. Wiscombe, *Appl. Opt.* **27**, 2502 (1988).
23. V. Boudon, M. Rey, M. Loëte, *J. Quant. Spectrosc. Radiat. Transfer* **98**, 394 (2006).
24. L. S. Rothman *et al.*, *J. Quant. Spectrosc. Radiat. Transfer* **82**, 5 (2003).
25. A. R. W. McKellar, *Icarus* **80**, 361 (1989).
26. E. Quirico, B. Schmitt, *Icarus* **127**, 354 (1997).
27. R. D. Lorenz, E. F. Young, M. T. Lemmon, *Geophys. Res. Lett.* **28**, 4453 (2001).
28. L. A. Mayo, R. E. Samuelson, *Icarus* **176**, 316 (2005).
29. O. B. Toon, C. P. McKay, R. Courtin, T. P. Ackerman, *Icarus* **75**, 255 (1988).
30. F. M. Flasar *et al.*, *Science* **308**, 975 (2005).
31. M. Fulchignoni *et al.*, *Nature* **438**, 785 (2005).
32. E. L. Barth, O. B. Toon, *Icarus* **162**, 94 (2003).
33. T. Tokano, *Icarus* **173**, 222 (2005).
34. W. R. Thompson, J. C. G. Calado, J. A. Zollweg, in *Proceedings of the First International Conference on Laboratory Research for Planetary Atmospheres*, Bowie State University, Bowie, MD, 25 to 27 October 1989 (NASA Conference Publication 3077, 1990), pp. 303–326.

35. This research was funded by NASA's Planetary Atmosphere Program (C.A.G.), the Brazilian Government's Coordenação de Aperfeiçoamento de Pessoal de Nível Superior scholarship, the Cassini Mission (P.P.), and the Portuguese Fundação de Ciência e Tecnologia scholarship SFRH/BD/8006/2002 (A.N.).

3 April 2006; accepted 25 July 2006
10.1126/science.1128245